

The Ofpe/WN9 stars in M 33 ¹

Luciana Bianchi

*Center for Astrophysical Sciences, The Johns Hopkins University, 239 Bloomberg Center
for Physics & Astronomy, 3400 N. Charles str., Baltimore, MD 21218, USA - Email:
bianchi@pha.jhu.edu*

Ralph Bohlin

Space Telescope Science Institute, 3700 San Martin Dr., Baltimore, MD 21218

Philip Massey

Lowell Observatory, 1400 W. Mars Hill Rd, Flagstaff, AZ 86001

ABSTRACT

We present HST/STIS Ultraviolet spectra of the six known Ofpe/WN9 stars (“slash stars”) in M 33. These stars were selected for showing the characteristics of the Ofpe/WN9 class from previous optical ground-based spectroscopy. The UV spectra are rich in wind lines, whose strength and terminal velocity vary greatly among our target sample. We analyse the STIS spectra with non-LTE, line blanketed, spherical models with hydrodynamics, computed with the WM-basic code. We find C to be underabundant and N overabundant, respect to the solar values, with a ratio (by mass) of C/N between 0.02 to 0.9 across the sample. Some stars show very conspicuous wind lines (P Cygni profiles), while two stars have extremely weak winds. The mass-loss rates thus vary greatly across the sample. The mass-loss rates of the hottest stars are lower than typical values of WNL stars, but higher than expected for normal population I massive stars. There is indication that the mass-loss rates may be variable in time. The C/N ratio, and the other physical parameters derived by the spectral modeling (T_{eff} , L_{bol} , mass), are consistent with evolutionary calculations for objects with moderately high initial masses ($\approx 30\text{-}50M_{\odot}$), evolving towards the WNL stage through an enhanced mass-loss phase.

Subject headings: Stars: abundances — Stars: early-type — Stars: evolution — Stars: fundamental parameters — Stars: mass-loss

1. Introduction

There is a general consensus about the Wolf-Rayet stars being formed from O stars through high mass-loss phases, but many specific questions remain still open. The Ofpe/WN9 stars (“slash stars”) class, introduced by Walborn (1977, 1982a), shows properties intermediate between those of Of and WN stars: the emission is stronger than in the most extreme Of stars, but HeII photospheric absorption indicates a less dense wind than seen in any Wolf-Rayet stars (see Bohannan & Walborn 1989). The implication is that Ofpe/WN9 stars are transition objects between the Of stars and the Wolf-Rayet in the “Conti scenario” (Conti 1976; Conti & Bohannan 1989). Based on the reduced surface H fraction observed in these stars, Pasquali et al (1997) suggest instead the sequence $O \rightarrow Of \rightarrow H\text{-rich WNL} \rightarrow Ofpe/WN9$, for initial masses less than $100 M_{\odot}$. One of the prototypes of the Ofpe/WN9 stars, R127 (HDE 269858) underwent an “S Dor like” eruption in 1982 (Walborn 1982b; Stahl *et al.* 1983) revealing Luminous Blue Variable (LBV) characteristics. Other evidence suggests that at least some of the Ofpe/WN9 stars have progenitors that are considerably lower in mass than the WNLs; see Massey, DeGioia-Eastwood, & Waterhouse (2001). LBV’s irregular episodes of extreme mass-loss may play an important role in the formation of W-R stars by substantial shedding of the progenitor’s outer layers (e.g. Maeder & Conti 1994).

Ten “slash stars” are known in the LMC (Bohannan & Walborn 1989). Seven LMC Ofpe/WN9 stars were investigated in the optical (Nota et al. 1996) and in the UV with Faint Object Spectrograph (FOS) spectra (Pasquali et al. 1997), and with IR spectroscopy by Morris et al (1996). The spectral morphology confirms the transition nature of these objects and their resemblance to LBVs. Crowther et al. (1977) also analysed optical spectra of LMC Ofpe/WN9 stars and re-classified them as WNL. Krabbe et al. (1991) observed a number of HeI emission line stars in the Galactic Centre, whose HeI line ratios and line-to-continuum ratio are consistent with Ofpe/WN9 stars. An Ofpe/WN9 star in NGC 300 was reported by Bresolin et al. (2002).

With follow-up, ground-based (KPNO, MMT) spectroscopy of about 400 UV-brightest stellar sources found in the *Ultraviolet Imaging Telescope* (UIT) far- and near-UV images of M 33, we discovered six Ofpe/WN9 stars in this galaxy (Massey et al. 1996, hereafter MBHS). The “slash stars” are UV bright. In our study of the UIT UV-brightest sources in M 33, these stars are relatively well separated from other stars in the $U - B$ vs. $FUV - NUV$ color-color diagram. They lie near the LBV candidates. Their colors are consistent with the fact that the Balmer jump is in *emission* in Ofpe/WN9 stars, which requires both high UV

¹Based on observations with the *Hubble Space Telescope* which is operated by AURA, Inc. under NASA contract NAS5-26555

flux and an extended atmosphere, consistent with the strong P Cygni profiles (e.g. HeI λ 4471) characteristic of the Ofpe/WN9 class.

We present *Space Telescope Imaging Spectrograph* (STIS) ultraviolet spectra of the six known Ofpe/WN9 stars in M 33. In section 2 details are given about the observations and the reduction, in section 3 the STIS UV spectra are analysed with non-LTE, line blanketed, hydrodynamical, spherical model atmospheres to derive physical stellar parameters. The results are interpreted in terms of stellar evolution by comparison with evolutionary model predictions (Section 4).

2. The program stars. Data and reduction

2.1. The program stars

In Bianchi’s HST program GO8207, we obtained UV spectra of the six Ofpe/WN9 stars known in M33. The spectra are shown in Figure 1. The objects were classified as Ofpe/WN9 from ground-based (KPNO, MMT) classification spectra of the UV-brightest stellar sources measured in the UIT far-UV and near-UV images (MBHS). The optical spectra, taken several years earlier (1993 - 1995), are shown in Figure 2 for the purpose of discussion in the following sections. A seventh object (M33-UIT339) was included in our program because of its photometric properties (H α emission-line source). An additional object, M33-UIT340, was included serendipitously in the STIS long slit during the M33-UIT339 observations by choosing an appropriate orientation. Its spectrum has a UV flux level comparable to the primary target, but much stronger UV lines, in spite of the similar optical colors. Another serendipitous star was observed due to failure of the acquisition on a repeated observation of M33-UIT349.

Data from our previous ground-based photometry are compiled in Table 1. In the table we give the star name, coordinates and V-mag, from the UIT sources list of MBHS. Also, for the position of every star we computed the de-projected galactocentric distance, using PA = 22° for the position angle of the semi-major axis of M 33, an inclination of the disk $i=54^\circ$ and a systemic velocity for M33 of $V_{sys}=-180 \text{ km s}^{-1}$ (from Warner et al. 1973). Warner et al. (1973) also provide a model for the rotation of the M33 disk from HI measurements. We computed the expected disk velocity, projected along the line of sight, at the position of each star. Because the targets are likely to lie in the M 33 disk, we used this velocity to shift the spectra to a rest-wavelength frame at the star. The position of the stellar lines indicates that this velocity correction is appropriate in all cases, although the difference from just using the M33 systemic velocity is not really appreciable at the resolution of our spectra. Both

the galactocentric distance and the recessional velocity are also given in Table 1. Finally, the STIS datasets are listed.

2.2. STIS spectroscopy and data reduction

The observations were completed over a long time span, because the HST entered a safe mode event just after our program (GO8207) began, and most of the observations were delayed because we missed the window for the desired orientation constraints. To assure homogeneous data quality and consistent flux calibration, we used the most recent on-the-fly calibration for all of the data after the program was completed.

For each star the same observing pattern was repeated: after target acquisition, a 24 min. long exposure was obtained with the STIS G230L grating (range 1570-3180 Å, scale 1.58Å/ pixel), followed by an 8 min. exposure in the same orbit with the grating G140L (range 1150-1730Å, scale 0.60Å/pixel). The whole subsequent orbit was devoted to a long (57 min) G140L exposure. The total exposure time was therefore 3300sec (G140L grating) and 1440sec (G230L grating) for every target. The STIS 0.2" x 52" slit was used. For target M33-UIT349, which is fainter than the others in the sample, we repeated this pattern twice, aiming at doubling the total time and achieve a S/N comparable to the other sample objects. The two sets of observations were taken about a week apart (Dec. 19 and Dec. 27, 2000). The spectra are significantly different on the two dates, both in flux level and wind lines, as can be seen in Fig 1. After examining the STIS CCD50 acquisition images, we discovered that the intended target (M33-UIT349) was actually observed on Dec. 27, while a nearby star was centered in the aperture on Dec. 19, during the fine centering stage, in spite the right target was exactly centered (on the same pixel) after coarse acquisition on both dates, as shown in Figure 3. We measured photometry on both dates, on the STIS CCD acquisition images: the two stars are equally bright in the CCD50 filter. Additionally, the target (M33-UIT349) appears slightly elongated in the acquisition images (Figure 3), but it is not clearly resolved into multiple sources. A cut of the long slit 2D spectra along the spatial direction, by summing several columns across the wavelength dispersion (Figure 4), shows a hint of a faint extension in M33-UIT349 spectrum (Dec. 27, datasets O5CO07010,20,30), although the two peaks, or asymmetric intensity profile, may just be an effect of the low countrate. The STIS MAMA spatial scale is 0.025"/pxl, and the width of the entire spectrum (see Figure 4) is about 10 pixels or .25", with the two brightest components less than .1" apart. Therefore it appears that, although the object is not resolved into multiple stars in the STIS CCD, which has a factor of two lower resolution than the MAMA, there may be some [marginal] extra light into the STIS slit from other fainter sources. The spectra are centered

in the y-direction (perpendicular to the dispersion) in the nominal position. Just based on the elongation seen on the finding chart, and the two apparent peaks in the spectrum intensity profile, we can speculate: could the object be a binary (multiple?) system, or is there a chance superposition of a faint source? A separation of $\leq 0.1''$ at the distance of M33 (840,000 pc, Magrini et al. 2000) would correspond to ≤ 0.4 pc, extremely large for a bound binary. An additional source seem to be excluded by the quantitative modeling of the spectra.

We will call the serendipitous star which was in the slit on Dec. 19, M33-UIT349-B hereafter. In the acquisition image, it is just $1.33''$ east of the target, thus the coordinates given in Table 1 are relative to the ground-based coordinates of the source (+0.10 seconds in R.A.). Most likely, the ground-based coordinates of M33-UIT349 were an intermediate position between the two sources, whose separation of $1.3''$ is not resolved in the ground-based image, and is comparable to the coordinate accuracy. The two stars can uniquely be identified from their relative positions and our finding chart (Figure 3).

For every target star we examined the two G140L exposures taken in subsequent orbits, and found that they perfectly match in absolute flux and the strong line features reproduce very well - in spite of the very different S/N due to the different exposure time. Also, we verified that the G230L and G140L fluxes match in the wavelength region of overlap. With the exception of M33-UIT339 (see later), we then combined the two G140L exposures, taking into account the different exposure times, to obtain the maximum possible total S/N over the range. The STIS flux calibration is expected to be accurate for sources in the broad $2''$ wide slit to 2% (Bohlin 2000; Bohlin, Dickinson, & Calzetti 2001). For the $0.2''$ slit used in this program, photometric precision of one wavelength with respect to a distant wavelength is 4.5% rms (Bohlin & Hartig 1998). There are no known non-linearities in the response of the STIS MAMA detectors. However, additional uncertainties arise from the Poisson counting statistics and from possible errors in background subtraction for the faintest sources.

An additional target, M33-UIT339, was included in our program GO8207 as it appeared to be an H α emission-line source, however it was not subsequently classified as an Ofpe/WN9 star. With an appropriate orientation, the STIS long slit centered on M33-UIT339 included also M33-UIT340, separated by about $4''$. The pipeline automatic extractions for the two G140L spectra, taken in subsequent orbits, are centered on the two different stars respectively, therefore the extracted spectra from the archive should *not* be used. The automatic pipeline extraction has centered the extraction slit on the target in one case (dataset O5CO03020), and on the serendipitous star in the other case (dataset O5CO03030). Therefore we manually re-extracted the spectra of both stars in all three exposures (two G140L and one G230L) and coadded them separately. While there is no acquisition image for the

second orbit (only reacquisition of previous guide stars was performed), we did obtain a parallel WFPC2 image with the same filter (F170W) in each orbit, as well as with different filters. Our F170W WFPC2 images with $0.1''$ resolution show that there is no shift between the two pointings down to the pixel level. The continuum level is the same over most of the G140L range, but the wind features are completely different for the two stars (Figure 1).

The spectra of the serendipitous stars are shown in Figure 1 for completeness, and for clarification of all acquisition and multiple-source issues to potential archive users. They will be analyzed separately.

Because the targets were selected from ground-based photometry and spectroscopy, we examined all the STIS acquisition images to check for multiplicity that might be revealed at the HST STIS imaging resolution but not in the ground-based data. All targets appear point-like.

3. Analysis of the UV spectra

3.1. UV line morphology

The short wavelength ($< 1750\text{\AA}$) portion of the spectra for all the program stars and the serendipitous stars is shown in Fig. 1. This wavelength region is richest in lines from the stellar wind (and the interstellar medium). The main wind lines are shown in detail in Figure 5, where their extent in velocity (largely varying across the sample) can be appreciated. The spectra are arranged from top to bottom of the figures in a progression of decreasing strength of the UV lines and decreasing wind velocity (width of the P Cygni absorption). Previous ground-based spectroscopy from MBHS also showed a range of line strengths within the sample. However, the progression is different from what the recent UV spectra indicates. The optical spectra from MBHS are shown in Figure 2. For example, M33-UIT008 was a weak-liner in the optical spectra, but displays some of the strongest UV features in the STIS spectra. Viceversa, M33-UIT349 has fairly strong optical lines (Figure 2), but not in the UV spectra. As another example, M33-UIT045 has weak lines both in the old optical spectra and in the UV spectra.

The UV line strength progression indicates a range of T_{eff} (luminosities) and mass-loss rates among the sample. It is difficult to relate the progression to an evolutionary sequence, because the relative line strengths are different between the optical spectra (≈ 1993 -1995) and the recent (2000-2001) UV spectra, suggesting variability. One stellar parameter which can plausibly vary on very short time-scales is the mass-loss rate, if these objects were single stars. Or are they evolved binaries? The quantitative spectral modeling described below is

aimed at clarifying the evolutionary status, by measuring the stellar parameters.

3.2. NTLE modeling with WM-basic

We performed detailed quantitative modeling of the spectra with the WM-basic code (Pauldrach et al. 2001). The code solves the wind hydrodynamics equations for specified parameters and includes non-LTE metal line blanketing in spherical geometry. It also allows us to include the effects of shocks (from clumps) on the wind ionization in the radiative transfer calculations, which are extremely important for a correct modeling of hot massive stars (e.g. Bianchi & Garcia 2002, 2003). Below we discuss the determination of the physical parameters for each individual star and how the uncertainties were estimated. More discussion on the uncertainties can be found in Section 4. The parameters from the best fit models are listed in table 2. The process is quite complex, given the many physical parameters which affect the emerging spectrum. The analysis of the first object is thus described in detail as a sample case. The effects of the physical parameters on the emergent spectrum are similar for the other objects. Initial guesses for the terminal velocities were taken by measuring the maximum extent of the P Cygni profile absorptions, which largely varies across the sample as can be appreciated (on an expanded scale, and independent of any modeling) in Figure 5.

3.2.1. *M33-UIT236*

The UV spectrum of this object indicates that it might be the hottest of the sample, and that it has a high mass-loss rate, because it has the strongest UV wind lines. We ran a grid of WM-basic models, with initial parameters covering a range of values for T_{eff} , luminosity and mass-loss rate inferred from a wider grid computed for other purposes. We computed synthetic model spectra for both solar and LMC-type metallicities, and then we also varied individual abundances of the CNO elements. In Table 2 we give the resulting stellar parameters and their uncertainty range, and here we discuss how they were constrained.

Before we discuss the strong P Cygni profiles that primarily constrain the main stellar parameters, we note that all models of the initial grid computed for LMC-type metallicity ($z=0.008$) are “flatter” than the observed spectra in the some spectral regions which contain no single strong lines, but a multitude of fainter lines, mainly from Fe III and Fe IV transitions (e.g. from 1420 to 1500Å). In these regions, the emerging flux in the low (LMC-type) metallicity models is close to a pure continuum, while the observed spectrum definitely shows shallow but significant depressions. These can be reproduced better in models with

solar metallicity ($z=0.02$). A precise determination of z is not possible. Therefore we adopted solar metallicity in the subsequent computation of the finer grid which includes the best fit adopted solutions, discussed hereafter. The result is not surprising given the metallicity gradient in M33 and that M33-UIT236 is relatively close to the galaxy center. The model spectra are sensitive to this effect only for large wind velocities.

The STIS spectrum of M33-UIT-236 (Figure 1) shows strong P Cygni profiles of both Si IV and N V, as well as a strong C IV $\lambda\lambda$ 1548,1551 doublet and C III multiplet around 1174Å. To reproduce the observed strength of both N V and Si IV consistently, we need to take into account the X-rays produced by shocks in the wind as a relevant ionization process. Because there is no prior information, to our knowledge, about soft X-ray emission from these objects, we tried a range of values that would be appropriate for early type luminous stars as observed e.g. in our Galaxy (e.g. Bianchi 1982a,b, Bianchi & Garcia 2002a,b). We found that for $T_{\text{eff}}= 32000$ K or lower, $L_x/L_\odot \approx -7$ is appropriate to reproduce the strength and shape of the N V doublet and the other “hot” transitions relative to the lines from lower ionization potential stages such as Si IV. A lower X-ray luminosity of $L_x/L_\odot=-7.5$ is found to be adequate at a higher T_{eff} (34,000K). The Si IV $\lambda\lambda$ 1394,1403 doublet, as well as N IV λ 1718, is not very sensitive to the effect of shocks, but is instead very sensitive to T_{eff} (especially in the range 34000 - 30000 K) and to the mass-loss rate. HeII λ 1640 is very sensitive to the mass-loss rate, in this temperature regime, thus cannot be used to constrain the helium abundance. The *relative* strength of the C IV to C III lines is again best reproduced by models between $T_{\text{eff}}= 32000$ K and $T_{\text{eff}}= 34000$ K. However, both of these C lines are always too strong for all parameter combinations which can reproduce the overall spectral features, in the models with solar abundances. We have therefore progressively decreased the C abundance (and changed correspondingly the abundance of N and O as expected in different evolutionary scenarios) and finally achieved a consistent fit of all the strongest wind lines with carbon 20 times less abundant than the solar value and nitrogen 10 times overabundant. These values correspond to the abundances predicted by evolutionary models for e.g. a star with initial mass of $\approx 30-50M_\odot$ reaching the WNL stage. The evolutionary models also predict oxygen to be underabundant by a factor of ten with respect to solar, and He/H up to 0.5 for evolved massive objects reaching such C and N abundances (e.g. Maeder 1987, Maeder & Meynet 1994, 2000, 2003). We thus adopted also [O]=0.1 the solar value, for consistency with our findings of the C and N abundances, although there are no strong oxygen lines in the range covered by our STIS spectra for stars in this temperature range to directly measure the oxygen abundance.

We varied He/H from 0.1 to 0.5 (by number) and in both cases we can achieve an acceptable fit of the overall spectrum, by slightly tuning the other parameters. Best fits are obtained with $T_{\text{eff}}= 32000$ K if He/H = 0.1 and with $T_{\text{eff}}= 34000$ K for He/H = 0.5.

Changing the helium abundance does not only affect the strength of the He II λ 1640, but also influences the relative strengths of other lines as well. Therefore we consider the actual helium abundance a source of uncertainty and adopt the above range for T_{eff} .

Once the *strength* of all P Cygni lines in the spectrum was matched by the models and the acceptable ranges constrained, we fine-tuned the trough of the absorptions, especially the Si IV doublet which is partly resolved. We varied both the terminal velocity and the rotational velocity. While the terminal velocity significantly affects the separation of the two absorption components of the Si IV doublet, and its uncertainty range is easily determined (see Fig. 5 and Table 2), rotational velocities of $V \sin i = 60 \text{ km s}^{-1}$ and twice as high $V \sin i = 120 \text{ km s}^{-1}$ were tested in the model calculations: the change only slightly affects the shape of the absorption troughs. This analysis is not as sensitive to this parameter ($V \sin i$) as the optical photospheric lines, since lines at UV wavelengths are mainly produced in the wind thus broad and asymmetric, and the STIS spectra resolution is too low for this purpose. The fit of the C III and Si IV lines, favours the high rotation. Again, a quantitative determination of this parameter is not possible; we can only infer from the comparison an indication of possible high rotation.

All the best fit models shown are computed with $\log g = 3.2$. The low gravity value was initially driven by the intention to compute models with reasonable mass/radius/luminosity values for this type of stars. We then tried higher gravities and obtained worse line fits. Note the good match of both the absolute flux values (a further confirmation that our choice of the Radius in the best fit models is adequate) and of the slope of the spectrum, independently confirming the temperature derived above by fitting the line strengths, and the extinction value (which is also consistent with the previous work of MBHS). Because the spectral slope depends on T_{eff} (and reddening) and the absolute flux depends on R^2 and T_{eff}^4 , the overall match to both the line profiles and the absolute flux level confirms the consistency of the parameters derived from our analysis.

The derived C/N ratio (by mass) of 0.02 is significantly lower than the cosmic value (4.8) and in the range of the WNL type stars (see e.g. Massey 2003). The C/N value is consistent, according to the stellar evolution calculations of Maeder (1987), Maeder & Meynet (1994), Meynet & Maeder (2000, 2003) with the surface abundances of a massive star during the stage from B supergiant to WNL. The current mass, T_{eff} and luminosity derived from our spectral modeling for M33-UIT236 agree with the evolutionary models for an initial mass of about $50 M_{\odot}$.

3.2.2. M33-UIT008

If we superimpose the spectrum of this star to the previous one (M33-UIT236), the two spectra, normalized to the respective continua, are basically identical except for much weaker nitrogen lines in M33-UIT008. In particular, the C IV and C III lines are identical, and so is the Si IV doublet, except for a clearer separation of the two absorption components, indicating slightly lower terminal velocity or mass-loss in M33-UIT008. He II λ 1640 is also identical. However, the N IV and N V lines are both significantly weaker than in the previous star. We attempted to explain this difference by either a lower nitrogen abundance or by a lower T_{eff} or \dot{M} . In our grid of models for solar CNO abundances, the N IV λ 1720 line becomes very weak (comparable to the one seen in the M33-UIT008 spectrum) when T_{eff} is cooler than 28000 K, for mass-loss rates of 3-5 $10^{-6} M_{\odot} \text{ yr}^{-1}$, but the strength of this line also decreases significantly with decreasing mass-loss rate. However, these models with lower T_{eff} produce too much Si IV and too little C III, respect to the observed spectrum, if we keep the other parameters similar to M33-UIT236, including the CNO “WNL-type” abundances. In short, a good fit of the other lines cannot be achieved at such low T_{eff} .

The strength of the N V doublet significantly decreases in models with lower L_x/L_{\odot} , however N IV is practically not affected by this change and the Si IV doublet is significantly enhanced. Therefore, varying this parameter does not produce a good fit either.

Because both N IV and N V transitions are weaker in UIT008 than in UIT236, but the spectra are otherwise identical, we computed models with the same parameters as the best fit of M33-UIT236, but lowered the nitrogen abundance from “WNL” values down to the solar value. This produces slightly lower (not lower enough) nitrogen lines but enhances the Si IV and C IV emissions enormously. Probably because we keep other parameters (such as mass-loss rate) the same, the opacities are redistributed. We also tried to decrease the mass-loss rate, and alter other parameters including different combinations of abundances, and the amount of shocks.

The best fit, in terms of the relative line strength and match to the flux below 1700Å, is achieved with the parameters given in Table 2. The results indicate that the main difference with respect to M33-UIT236 is a lower mass-loss rate.

We caution that Bianchi & Garcia (2002), Garcia & Bianchi (2003) encountered some difficulties in fitting weak N V lines in pop. I Milky Way stars with the WM-basic code, and better matches could be achieved in some cases using Hillier’s CMFGEN code, although the resulting stellar parameters were not changed (e.g. Bianchi et al. 2003a, b). Therefore, the derived abundances, in particular of N in this case, must be taken as indicative, as stressed in the previous section.

3.2.3. M33-UIT104

The *line* spectrum suggests lower wind velocity and a lower stellar temperature than the previous stars examined, the “cooler” transitions (C III and N IV) being enhanced and the higher ions (N V and C IV) weaker. A similar effect on the line strength, to some extent, may be produced by a lower amount of X-rays from shocks. All these effects were quantified by the modeling (Table 2). A CIII line, visible as a small but detectable absorption in the emission of N V, is the most unambiguous indication of $T_{\text{eff}} \leq 32000$ K according to our grid of models (see Bianchi & Garcia 2002), at least for solar abundances. Therefore, this line provides a strong constraint on T_{eff} .

In this T_{eff} regime, the C III 1175Å line becomes much more sensitive to the C abundance than to the mass-loss rate (while C IV is saturated so rather insensitive to all parameters). This is very fortunate because it allowed us to constrain one parameter (the C abundance) relatively independently from the other ones in this case. Along the stellar evolution, the C-depletion develops concurrently with the N-enrichment (according to Maeder 1987), therefore we tried different abundance ratios for C and N, corresponding to a typical predicted evolutionary sequence. The best fit is shown in figure 6, and was achieved with [C]=0.1 x solar and [N]=2 x solar. In mass fraction, this means C/N=0.9.

Again the match to both the line strength and to the absolute flux level, and the continuum shape, is very good shortwards of 1700Å.

3.2.4. M33-UIT003, M33-UIT349 and M33-UIT045

Continuing towards progressively weaker P Cygni profiles and lower terminal velocities, M33-UIT003, M33-UIT045 and M33-UIT349 (Dec.27) show a smooth decrease in the lines of Si IV and C IV, compared to the previous targets. Instead, the N V $\lambda 1240$ doublet abruptly disappears in the spectra of M33-UIT045 and of M33-UIT349. In modeling the spectrum of M33-UIT045, it has been impossible to obtain a synthetic spectrum which matches the line features, and the absolute flux, with nitrogen abundance solar or higher. The best fit spectrum (shown in Figure 6) was obtained by lowering the nitrogen abundance by a factor of ten with respect to solar. A nitrogen underabundance in such evolved massive star is hard to explain and extremely suspicious. Again, we caution that model calculations may be less reliable for such extreme parameters than for the previous cases.

Similarly to M33-UIT045, it has been extremely difficult to produce a synthetic spectrum without N V to match the observed spectrum of M33-UIT349. The fit was achieved with an extremely low mass loss rate, about two order of magnitude lower than the other stars

in the sample. The result is consistent with the fact that the typical wind lines in the UV spectrum are almost absent. However, the low mass-loss rate is surprising since this star has photospheric parameters not too different from the rest of the sample. We must keep in mind that additional faint sources may contribute -although marginally - to the spectrum, but they are not resolved nor confirmed. It is also puzzling that the wind lines in the M33-UIT349 spectrum seems **wider** rather than narrower, compared to the spectra with stronger lines. Typically, a progression from stronger to weaker P Cygni profiles (i.e. decreasing mass-loss) also corresponds to decreasing wind velocities, as it evident e.g. in the sequence (from the top down) of spectra in Figures 1 and 5. The large velocity may suggest a physical binary, i.e. two stars with high ($\approx 1000\text{km s}^{-1}$) velocity relative to each other, both having weak lines. Or, more simply, the fact that the lines are so weak (and the limited S/N) prevents to resolve blends and makes the analysis inconclusive in this case.

Finally, for two “weak-lined” spectra, modeling was achieved with a carbon underabundance (respect to solar) of a factor of two, and not twenty like the hotter stars with stronger winds, and lower mass values. The derived parameters T_{eff} , L_{bol} , Mass, are again consistent with the evolutionary models of Maeder, since lower mass stars produce less enhancement of N and less depletion of C, than more massive stars.

Looking at the absolute flux level and slope at longer wavelengths (Figure 7), we note a slight mismatch between model and observed spectrum for M33-UIT008, M33-UIT045 and M33-UIT003. While the best fit model reproduces well the continuum and all the lines in the shorter wavelengths range (where the flux from the hot star dominates), the slope of the entire observed spectrum cannot be matched perfectly by any single star model for any combination of reddening (using known reddening types). The mismatch between model and observed spectra, however, is of the order of $0.1 - 0.2 \cdot 10^{-14}\text{ergs cm}^{-2} \text{s}^{-1}$, or \approx up to 5% beyond $\approx 1500\text{\AA}$, thus comparable to the calibration uncertainty. The flux level and the line spectrum are matched well in the short wavelength range, pointing to a consistent and plausible model fit for the hot star. In the finding chart produced from the STIS CCD acquisition image and the spectral intensity cuts shown in Figure 4, no extra faint components can be clearly resolved. Therefore, the mismatch could indicate either an unresolved chance superposition of a fainter cooler star (statistically unlikely), or a faint binary component with separation less than $\approx 0.2\text{pc}$ (unresolved), or an UV extinction slightly different than the types known so far in the MW or LMC (see next section). The level of mismatch is however of the order of the calibration accuracy (see Section 2.2.), therefore it could just be an instrumental effect.

4. Discussion and Conclusions

We analyzed STIS Ultraviolet spectra of six Ofpe/WN9 stars in M33. Previous optical spectra of our sample (MBHS) showed a progression from “weak-lined” slash stars, similar to BE470 in the LMC (with strong P Cygni HeI and Balmer emission but very weak NIII λ 4634,42 and HeII λ 4686) to “strong lined” slash stars, similar to BE381 in the LMC (with strong NIII and HeII). The UV line spectra show a progression (Figure 1) of line intensities which does not correlate with the earlier optical spectra (Figure 2), suggesting possible variability on short time-scale (years) of the mass-loss rate.

One target, M33-UIT349, was observed twice, 8 days apart, but successfully only on Dec. 27. Its spectrum seems to include a very faint extension (Figure 4), separated spatially by $<0.1''$ (thus if physically associated, by $<0.4\text{pc}$), but the source is not resolved into separate components at the STIS CCD resolution (Figure 3). In any case, the apparent secondary component has negligible flux with respect to the main source (figure 4), as confirmed by the good fit to the spectral distribution. The spectrum shows extremely weak wind lines.

For three stars (half of the sample) we find C/N=0.02 by mass, consistent with predictions from stellar evolution models for an evolved massive star (initial mass $\approx 40\text{-}50 M_{\odot}$) in the phase transitioning from Blue supergiant to WNL (i.e. towards the W-R stage) at constant luminosity in the H-R diagram. The other physical parameters (T_{eff} , mass, luminosity) are also entirely consistent with the scenario of massive stars approaching the WNL stage (Maeder 1987, Maeder & Meynet 1994, Meynet & Maeder 2000, 2003). It must be kept in mind that the available spectroscopic range provides several wind lines but no photospheric lines, therefore derivation of abundances is not very accurate as wind line strengths depend also on the mass-loss rate and other factors. However, the consistency of the entire modeling (lines, absolute flux, velocity) supports the results as quite reliable, and all the parameters indicate a consistent evolutionary picture. For the other three stars, C was found to be (by number), only about half the solar value. For M33-UIT104, the analysis indicates N to be overabundant by a factor of two, i.e. C/N = 0.9 by mass. For the other two stars with extremely weak lines, the nitrogen abundances and the overall modeling is way more uncertain, for the reasons explained in the previous section. Either these stars are in an earlier evolutionary stage, evolving off the ZAMS, still towards lower T_{eff} ’s, or their progenitors has lower initial masses (by comparison with Maeder’s evolutionary calculations). Variability of the mass loss rate is also possible, as mentioned, complicating the interpretation.

Studies of coeval clusters in the Milky Way (Massey, DeGioia-Eastwood, & Waterhouse 2001) and Magellanic Clouds (Massey, Waterhouse, & DeGioia-Eastwood 2000) suggest that LBVs are descendent from the most massive stars ($> 90M_{\odot}$). The two Ofpe/WN9 stars in their sample, however, come from stars of much lower mass, $> 25\text{-}35M_{\odot}$, calling into

question the evolutionary link between LBVs and Ofpe/WN9s. The range of progenitor masses inferred by comparing our derived current masses, abundances, T_{eff} and luminosities with evolutionary calculations ($\approx 30\text{-}50M_{\odot}$), is consistent with their findings. On the other hand, a link between LBVs and Ofpe/WN9 has been observationally established in the cases e.g. of AG Car, R127, S61, S119 (Stahl 1987, Stahl et al. 1983, Pasquali et al. 1999, Nota et al. 1995) although these studies do not provide enough statistics to quantify the correlation in terms of evolution. Langer et al. (1998) and Lamers et al. (2001) discuss the effect of stellar rotation, on the evolution of massive stars, and show that rotation ”extends” the occurrence of the LBV phase to lower progenitor masses.

One important parameter, the mass-loss rate, varies from $8 \cdot 10^{-6} M_{\odot} \text{ yr}^{-1}$ to $2 \cdot 10^{-6} M_{\odot} \text{ yr}^{-1}$ among the first four stars in table 2, which appear to have similar masses (within the uncertainty of our analysis) but a range of temperatures. The uncertainties on the mass-loss rates are less than 30% according to our model calculations. Although the difference in T_{eff} within our sample covers a fairly narrow range, and the sample is numerically limited, there is a trend of mass-loss increasing as the star evolves towards the W-R stage and becomes hotter. Mass-loss rate increases with luminosity (e.g. Bianchi & Garcia 2002, Nugis & Lamers 2000, Vink et al. 2001), but the small range of luminosity variation among the sample does not explain the large mass-loss rate spread (see below).

The values of \dot{M} that we derive for the “strong-lines” stars (the first four in Table 2) are lower than the high mass-loss rates of W-R stars, and higher than mass-loss rates expected for O stars with similar parameters. Maeder’s evolutionary models assume an average $\dot{M} = 4 \cdot 10^{-5} M_{\odot} \text{ yr}^{-1}$ for WNL stars, and the Nieuwenhuijzen & de Jager (1990) parametrization for the earlier stages (this parametrization is based on a compilation of observed mass loss rates). Our mass-loss rates are also lower than Nieuwenhuijzen & de Jager (1990) parametrization which, for the physical parameters given in table 2, would predict for the first four stars of the sample \dot{M} between 2.1 and $1.5 \cdot 10^{-5} M_{\odot} \text{ yr}^{-1}$. Recent works revised the mass-loss rates for Wolf-Rayet stars, taking into account “clumping” in the wind. These mass-loss rates are generally lower than earlier determinations, of the order of $\geq 1 \cdot 10^{-5} M_{\odot} \text{ yr}^{-1}$ for WN-type stars of comparable luminosities to our targets (Nugis & Lamers 2000; Nugis, Crowther & Willis 1998; Graefner, Koesterke & Hamann 2002), thus higher than what we measure for the Ofpe/WN9 stars. To compare with O-type stars, we use the recent “recipe” (based on theoretical monte-carlo simulations) from Vink et al. (2000, 2001), for pop.I stars, and find that the predicted mass-loss rates are of the order of $2 \cdot 10^{-6} M_{\odot} \text{ yr}^{-1}$ for the first five stars (2.4 to $1.7 \cdot 10^{-6} M_{\odot} \text{ yr}^{-1}$ from M33-UIT236 to M33-UIT045), for solar metallicity, and less for metallicity lower than solar (e.g. for $z=0.1 \times$ solar, \dot{M} would be lower by a factor of seven). In summary: the values of mass-loss rates derived for our sample are lower than typical W-R mass-loss rates, but in comparison to predictions from radiation-pressure wind

theory for pop.I stars, mass loss is enhanced for the hottest stars (M33-UIT236, M33-UIT008, M33-104), is comparable to the predictions for M33-UIT003, and lower than predicted for M33-UIT045 and M33-UIT349. However, as we stressed before, \dot{M} derivations are less reliable for the two latter stars, as the lines are extremely weak. Another result emerging by these comparisons is that mass-loss rate varies within the sample more than we would expect from the variation of the other physical parameters (T_{eff} , L_{bol} , mass). For this fact, and because the UV line strengths do not correlate with optical line strengths observed several years earlier, we suggest that mass-loss rate may vary in time as well. LBV stars also display variable mass-loss rates, which Vink & de Koter (2002) explain in terms of changes in the line driving efficiency. The large spread in mass-loss rates among our sample may also relate to evolutionary effects. The physical conditions of the radiation-pressure driven wind change during the evolutionary phases from O-type to LBV to W-R, and these classes of objects display very different mass loss rates and wind velocities, although the stellar luminosity remains basically constant during the transition. According to Lamers & Nugis (2002), the wind changes are mainly due to change in stellar parameters (radius, gravity) and to a lesser extent to change in surface chemical abundances. The ensemble of our findings consistently points out that the first four objects in Table 2 are transitioning towards the W-R (WNL) stage through an enhanced mass-loss phase.

All spectra are very well fitted in both continuum flux level and line strength at the short wavelengths (G140L range), while a mismatch between observed flux and model is seen longwards for most stars. All stars appear to be point-like sources at the STIS spatial resolution. The amount of the mismatch (up to 5% at the longer wavelengths) is comparable to the absolute flux confidence level (section 2.2), and to the uncertainty in the extinction amount and extinction law. A variation in $E(B-V)$ of 0.01 would have an effect comparable to the mismatch seen beyond 1700Å. However, it would create a larger mismatch at the shorter wavelength, which are more sensitive to the reddening, thus was excluded. The amount of extinction ($E(B - V)$) adopted as our best fit to the spectra is given in table 2, and the adopted extinction law is a combination of Galactic extinction (foreground) and LMC-type extinction. This was found to be generally the preferable solution, after examining different combinations with all known extinction laws (for other galaxies), concurrently with varying the stellar model parameters. The UV extinction law in M 33 is currently being investigated by us with another STIS program, and the results may refine this issue. We attempted to add different black-body components to the stellar-model fits. While we may visually improve the fit to the observed spectra at the long wavelengths, removing the mismatch, the results would not be significant given that the flux level of a postulated additional component would be up to a few % that of the luminous hot star. Therefore, we cannot conclude at this point, whether a faint excess flux, peaking at about 1800Å or longwards, is present in addition to

the brighter hot luminous star spectrum, or if the extinction curve slightly differs from the MW and LMC ones.

Finally, we point out again two remaining possible sources of uncertainty in the present analysis. The first may come from some inconsistency in the WM-basic calculations, for the cases of extreme parameters such as those of M33-UIT045 and M33-UIT349, where the flux indicates a hot, luminous object but the lack of wind lines (or just of NV in the case of M33-UIT045) indicates an unusually low mass-loss rate. These caveats are discussed at length by Bianchi & Garcia (2002,2003b), Garcia & Bianchi (2003). Second, the amount of shocks in the winds and the effect of the related X-rays on the ionization - which bears on the T_{eff} results, cannot be precisely estimated when only the UV range is available. The FUSE range, at shorter wavelengths, contains transitions much more sensitive to this parameter than those in our STIS spectra, primarily the O VI doublet (Bianchi & Garcia 2002, Bianchi et al. 2003). We plan to extend the analysis of the sample to the FUSE range as a next step, although the fluxes of these distant objects are at the limit of detection for FUSE.

It is interesting to compare our findings with similar objects in other galaxies, to verify metallicity effects on the evolution. To our knowledge, no similar modeling of UV spectra has been performed for Ofpe/WN9 stars in the MW or other galaxies. However, previous works, mostly based on optical spectroscopy, provide very useful comparisons. Similarly to our STIS spectra, UV FOS spectra of all the LMC “slash stars” show P Cygni profiles of CIII λ 1176, SiIV $\lambda\lambda$ 1394,1403 and NIII $\lambda\lambda$ 1748, 1752. Other strong lines, CIV $\lambda\lambda$ 1548,1550, NV $\lambda\lambda$ 1238,1243, HeII λ 1640, NIV λ 1719 and AlIII $\lambda\lambda$ 1855,1863, vary from pure absorption to strong P Cygni profiles in the sample (Pasquali et al. 1997). these authors derive terminal velocities of the order of 400 km s^{-1} , much lower than the wind velocities measured in our sample, and mass-loss rates (from H α equivalent widths) of $\approx 2 - 5 \cdot 10^{-5} M_{\odot} \text{ yr}^{-1}$, much higher than what we found for the M33 counterparts. The discrepancy may be due to the H α equivalent width method, where the correction for the underlying photospheric absorption is a very large source of uncertainty (Bianchi & Scuderi 1999). A non-LTE analysis of the optical spectrum of an Ofpe/WN9 star in NGC 300 was performed by Bresolin et al. (2001) using the Hiller & Miller (1998) code. The T_{eff} is lower, but the luminosity and the mass loss rate higher, than the range of values found in our sample. Crowther et al. (1977) performed a non-LTE analysis of optical spectra of LMC’s Ofpe/WN9 stars, which they however re-classified as WNL (WN9-11). They find a range of T_{eff} which overlaps with the lower end of our range, most of their sample (WN9-11) stars having lower T_{eff} ’s than ours, and higher \dot{M} values. We caution again that mass loss rates derived from UV and from optical spectra give often discrepant results (e.g. Crowther et al. 2002, Bianchi & Garcia 2002), thus the comparison has to be taken with caution. A more conclusive comparison would require similar analysis of similar data-sets.

Support for this work (proposal GO 8207) was provided by NASA through grant GO8207-0197A from the Space Telescope Science Institute, which is operated by the Association of Universities for Research in Astronomy, Inc., under NASA contract NAS5-26555. We are very grateful to Miriam Garcia for computing several WM-basic models of the grid used in this work, and to Jorick Vink, Lars Koesterke and Wolf-Rainer Hamann for useful discussions.

REFERENCES

- Bianchi, L., 1982a, ESA SP-176, p. 251
- Bianchi, L., 1982b, *Adv. Space Res.*, Vol.2, n. 9, p. 293
- Bianchi, L., 1995, *SEA Bulletin*, 6, 28
- Bianchi, L., & Scuderi, S. 1999, *Mem. SAIT*, 70 N.2, p. 667
- Bianchi, L., & Garcia, M. 2002, *ApJ*, 581, 610
- Bianchi, L., & Garcia, M., 2003, in "The Local Group as an Astrophysical Laboratory", in press
- Bianchi, L., Garcia, M., & Herald, J. 2003, *RMxAA*, 15, 226
- Bianchi, L., Garcia, M. & Herald, J. 2003b in preparation
- Bohannon, B. & Walborn, N.R. 1989, *PASP*, 101, 520
- Bohlin, R. C. 2000, *AJ*, 120, 437
- Bohlin, R. C., Dickinson, M. E., and Calzetti, D. 2001, *AJ*, 122, 2118,
- Bohlin R. & Hartig, G. 1998, *Instrument Science Report*, STIS 98-20, (Baltimore:STScI)
- Bresolin, F. Kudritzki, R.-P., Najarro, F. et al. 2002, *ApJ*, 577, L107
- Conti, P.S., & Bohannon, B. 1989, *IAU Coll.* 113, p.297
- Conti, P.S. 1976, *Mem. Soc. Roy. Science Liège*, 9 (6), 193
- Crowther, P. A., Hillier, D. J., Evans, C. J., et al. 2002, *ApJ*, 579, 774
- Crowther, P. A., & Smith, L.J. 1997, *A&A*, 320, 500
- Gräfener, G., Koesterke, L. & Hamann, W.-R. 2002, *A&A*, 387, 244
- Hiller, D. J., & Miller, D.L. 1998, *ApJ*, 406, 407
- Krabbe, A., Genzel, R., Drapatz, S., Rotaciuc, V. 1991, *ApJ*, 382, L19
- Lamers, H.J.G.L.M., & Nugis, T. 2002, *A&A*, 395, L1

- Lamers, H.J.G.L.M., Nota, A., Panagia, N., Smith, L.J., & Langer, N. 2001, 551, 764
- Langer, N., Heger, A. & Fliegner, J. 1998, IAU Symp. 189, 343
- Maeder, A. & Conti, P.S. 1994: ARA&A, 32, 227
- Maeder, A. 1987, A&A, 173, 247
- Maeder, A. & Meynet, G. 1994, A&A, 287, 803
- Meynet, G. & Maeder, A. 2000, A&A, 361, 101
- Meynet, G. & Maeder, A. 2003, A&A, 404, 975
- Magrini, L., Corradi, R., Mampaso, A. & Perinotto, M. 2000 A&A, 355, 713
- Massey, P. 2003, Ann. Rev. Astron. Astrophys. 2003, 41, 15
- Massey, P., Bianchi, L., Hutchings, J.B. & Stecher, T. 1996, ApJ, 469, 629 (MBHS)
- Massey, P., DeGioia-Eastwood, K. & Waterhouse, E. 2001, AJ, 121, 1050
- Massey, P., Waterhouse, E. & DeGioia-Eastwood, K. 2000, AJ, 119, 2214
- Morris, P.W., Eenens, P.R.J., Hanson, M.M., Conti, P.S., & Blum, R.D. 1996, ApJ, 470 597
- Nota, A., Pasquali, A., Drissen, L., Leitherer, C., Robert, C., Moffat, A., & Schmutz, W. 1996, ApJS, 102, 383
- Nota, A., Pasquali, A., Drissen, L., & Leitherer, C., Robert, C., Schmutz, W. 1995, ApSS 224, 261
- Nugis, T., & Lamers, H.J.G.L.M. 2000, A&A, 360, 227
- Nugis, T., & Lamers, H.J.G.L.M. 2002, A&A, 389, 162
- Nugis, T., Crowther, P., & Willis, A. 1998, 333, 956
- Pasquali, A., Langer, N., Schmutz, W., et al. 1997, ApJ, 478, 340
- Pasquali, A., et al. 1999, A&A, 343, 536
- Pauldrach, A.W.A., Hoffmann, T.L., & Lennon, M. 2001, A&A, 375, 161
- Stahl, O. 1987, 182, 229
- Stahl, O., Wolf, B., Klare, G., Cassatella, A., Krautter, J., Persi, P., & Ferrari-Toniolo, M. 1983, A&A, 127, 49
- Vink, J.S., de Koter, A., & Lamers, H.J.G.L.M. 2000, A&A, 362, 295
- Vink, J., de Koter, A., & Lamers, H.J.G.L.M. 2001, A&A, 369, 574
- Vink, J., & de Koter, A. 2002, A&A, 393, 543
- Walborn, N. 1977 ApJ, 215, 53

Walborn, N. 1982a, ApJ, 256, 452

Walborn, N. 1982b, IAU Circ. No. 3767

Walborn, N., Lennon, D., Haser, S., Kudritzki, R.-P., & Voels, S.A. 1995, PASP, 107, 104

Warner, P.J., Wright, M.C.H., & Baldwin, J.E. 1973, MNRAS, 163, 163

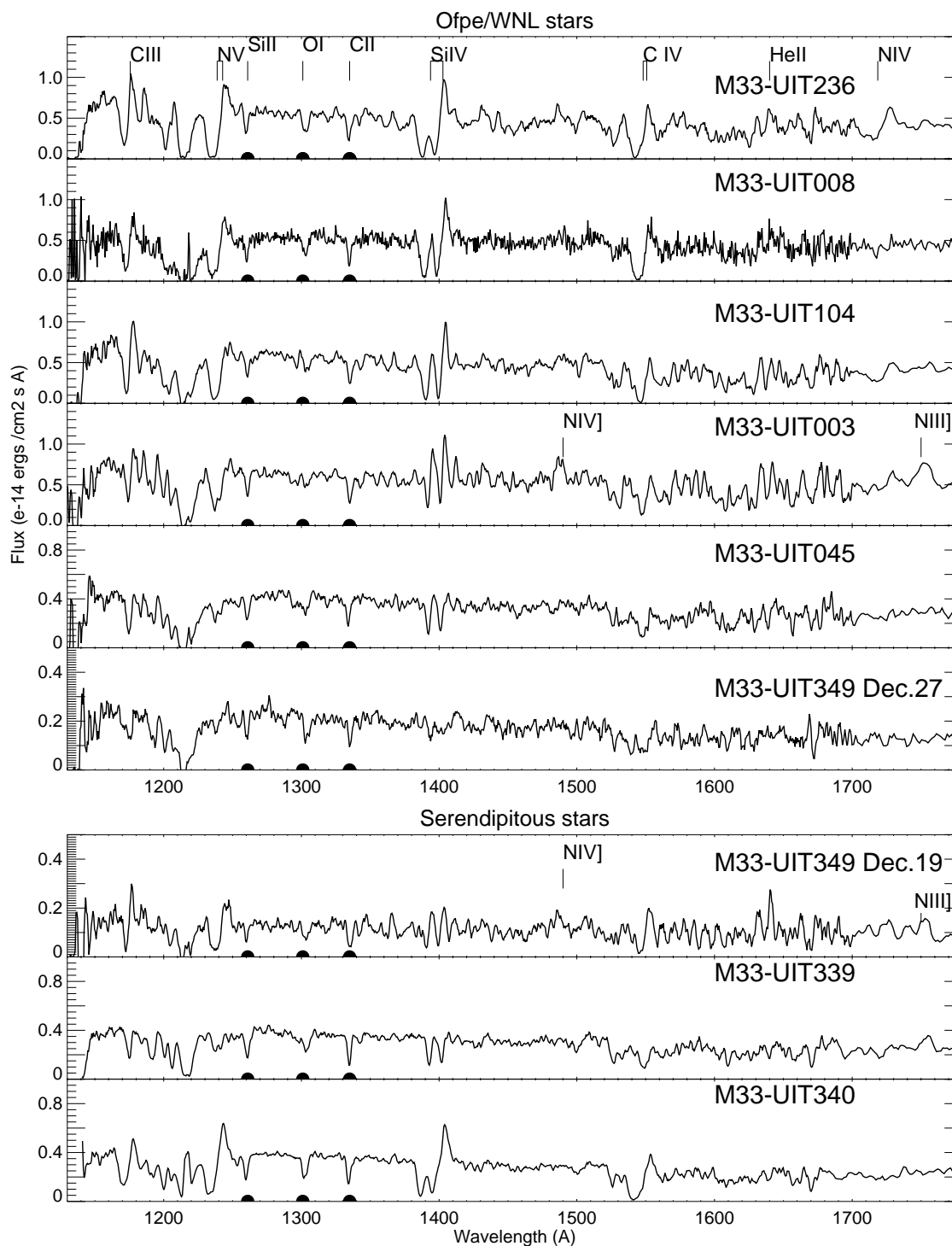


Fig. 1.— The UV spectra in the short wavelength range, which contains the lines of interest: CIII, CIV, NIV, NY, SiIV, HeII. The Ofpe/WN9 program stars are arranged by progressively decreasing strength of the UV wind lines. The spectra of the serendipitous stars (see text) are shown at the bottom. The strongest interstellar lines in this range, Si II λ 1260, O I λ 1301, and C II λ 1335, are marked with a filled bubble at the bottom of the spectra. The strongest stellar features are also marked on the top spectrum.

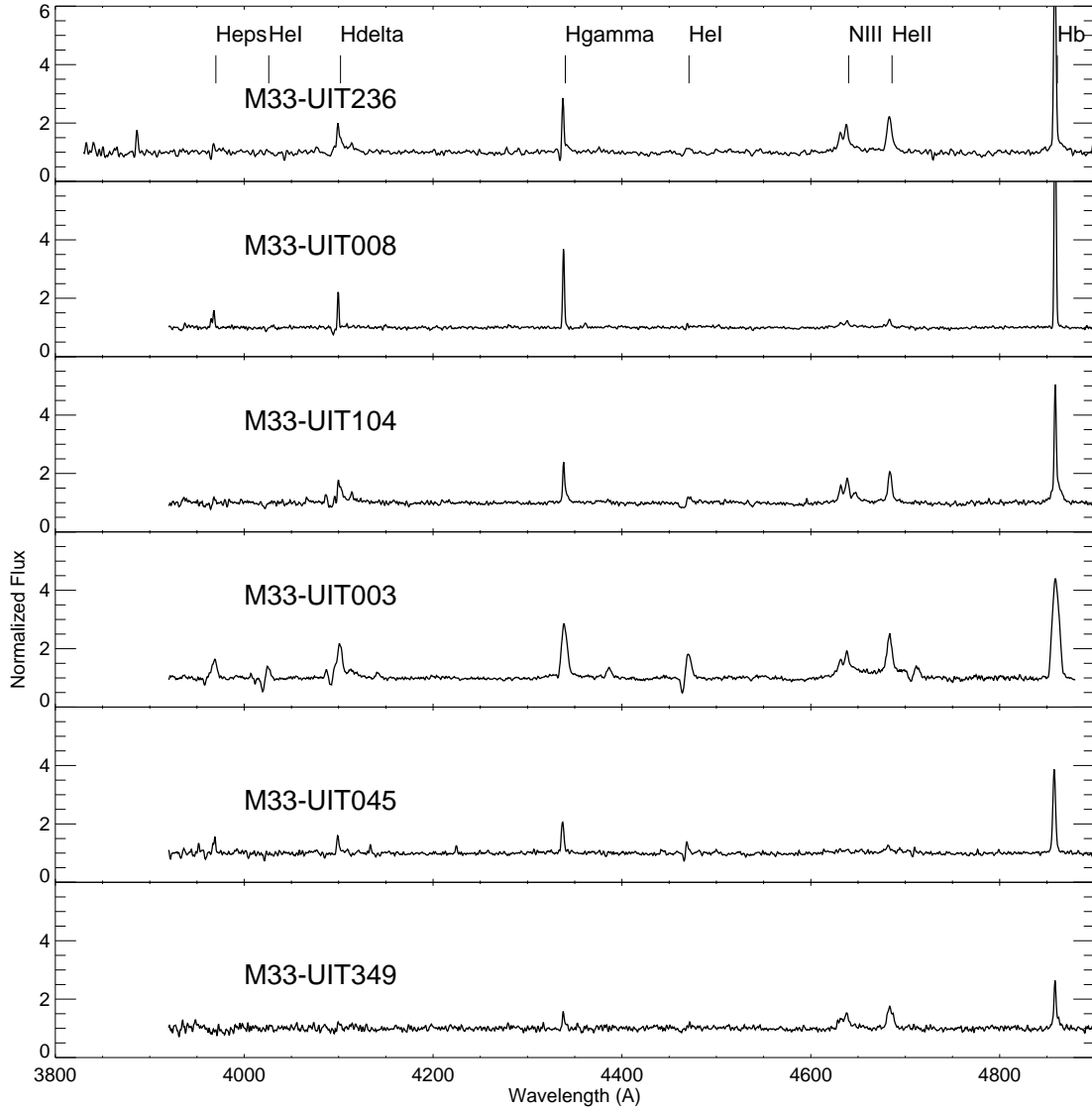


Fig. 2.— The optical spectra of the program stars (about 2\AA resolution, from MBHS), are shown arranged in the same order as the UV spectra in Fig. 1. To facilitate appreciation of relative line strength, the spectra are normalized to the continuum, and plotted on identical scale. The relative line strength does not match the progression seen in the UV lines, suggesting variability.

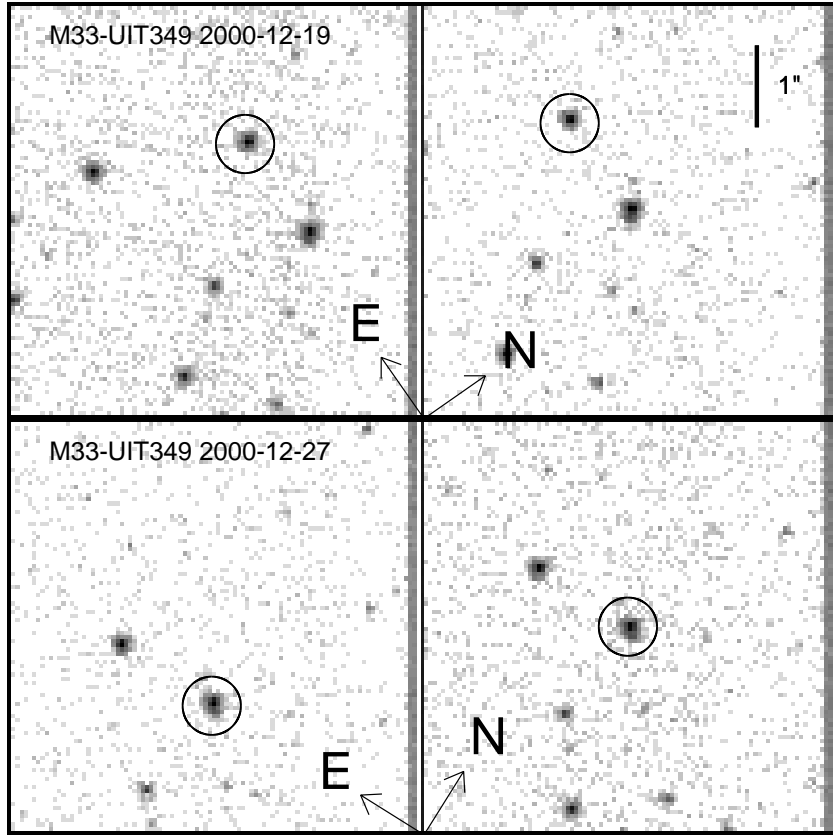


Fig. 3.— Acquisition images of M33-UIT349. Left: before centering - Right: after coarse acquisition centering. Note that the orientation is different on the two dates (PA=54.65 on Dec.19 and PA=31.64 on Dec.27). The target was acquired and perfectly centered in the coarse stage, on both dates, however on Dec. 19 during the fine acquisition there was a jump and another star of equal brightness (in the circle) was put in the slit.

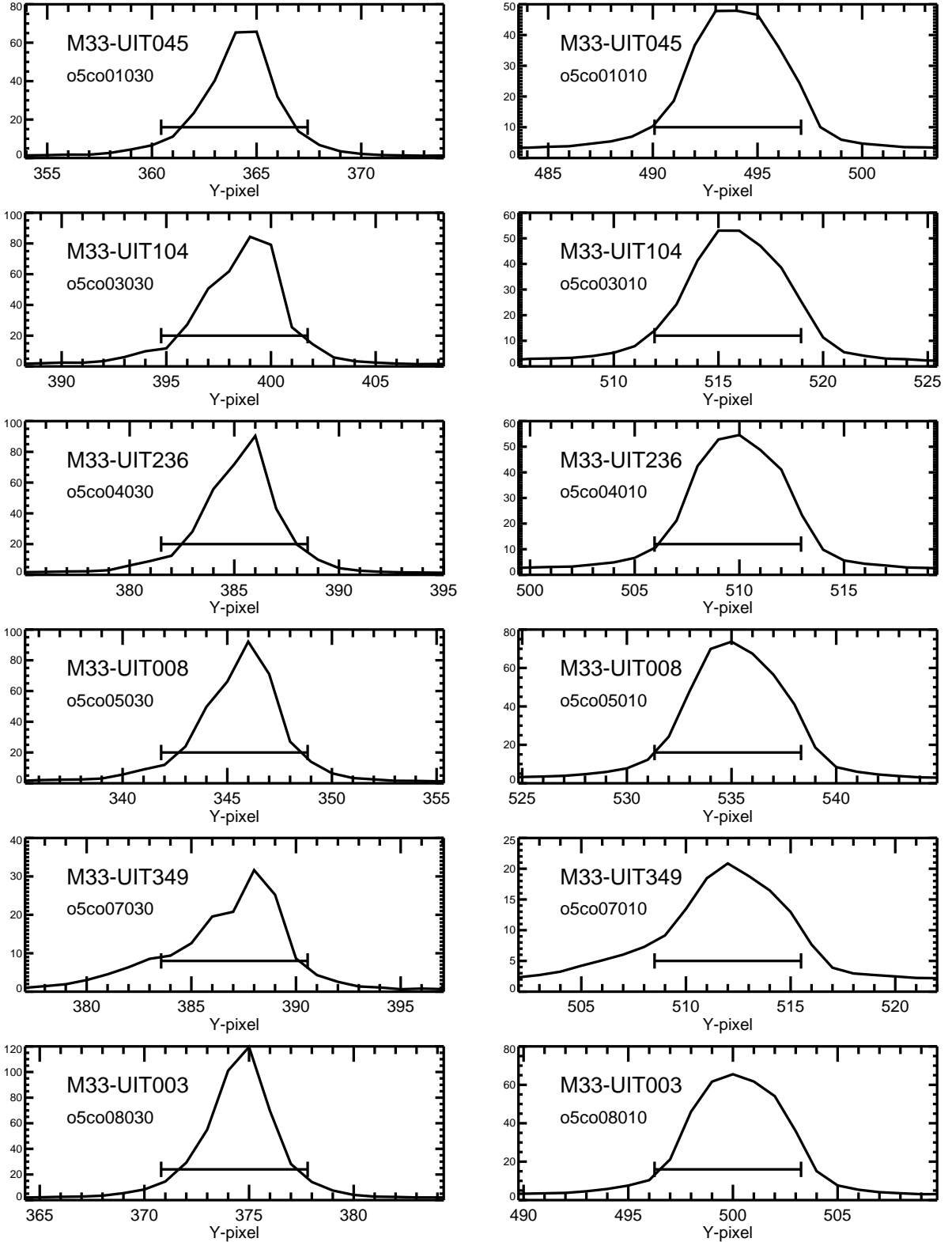


Fig. 4.— Intensity profile in the spatial direction for the G140L (left) and G230L (right) spectra. for all the program stars. The profile is the sum of 301 columns around the center of the image. The data shown for M33-UIT349 are the Dec.27 observations, when the correct target was observed.

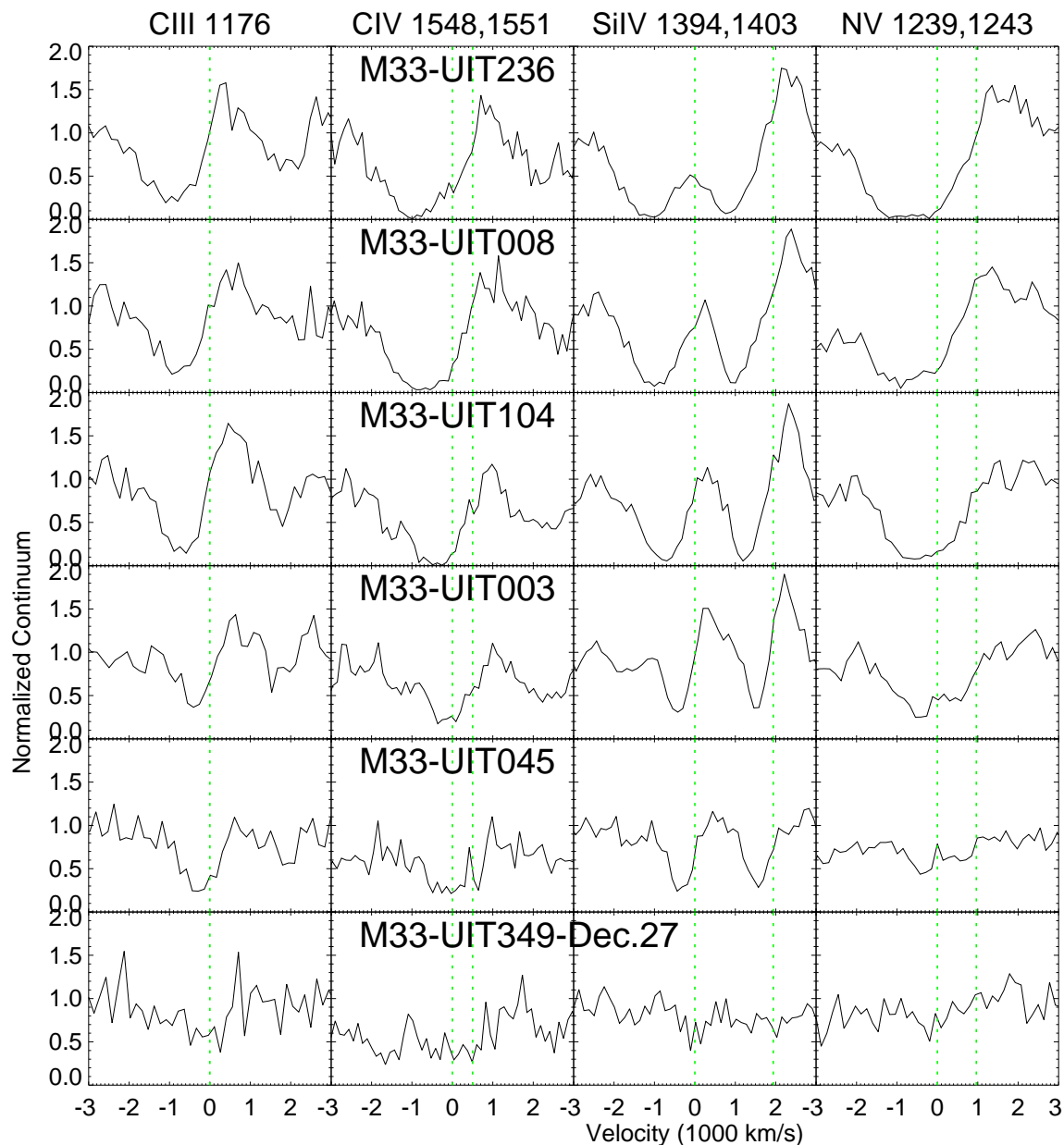


Fig. 5.— The four strongest UV wind lines are shown in velocity scale (thousand km s^{-1}) for the Ofpe/WN9 program stars. Vertical green (dotted) lines indicate the rest positions of the transitions. The recession velocity of each star (Table 1) has been removed. From top to bottom, the lines show a progression of decreasing strength and width (i.e. decreasing wind terminal velocity). The effect is especially evident in the Si IV doublet, where the two components are more separated in wavelength (while the C IV and N V doublets are always blended in velocity).

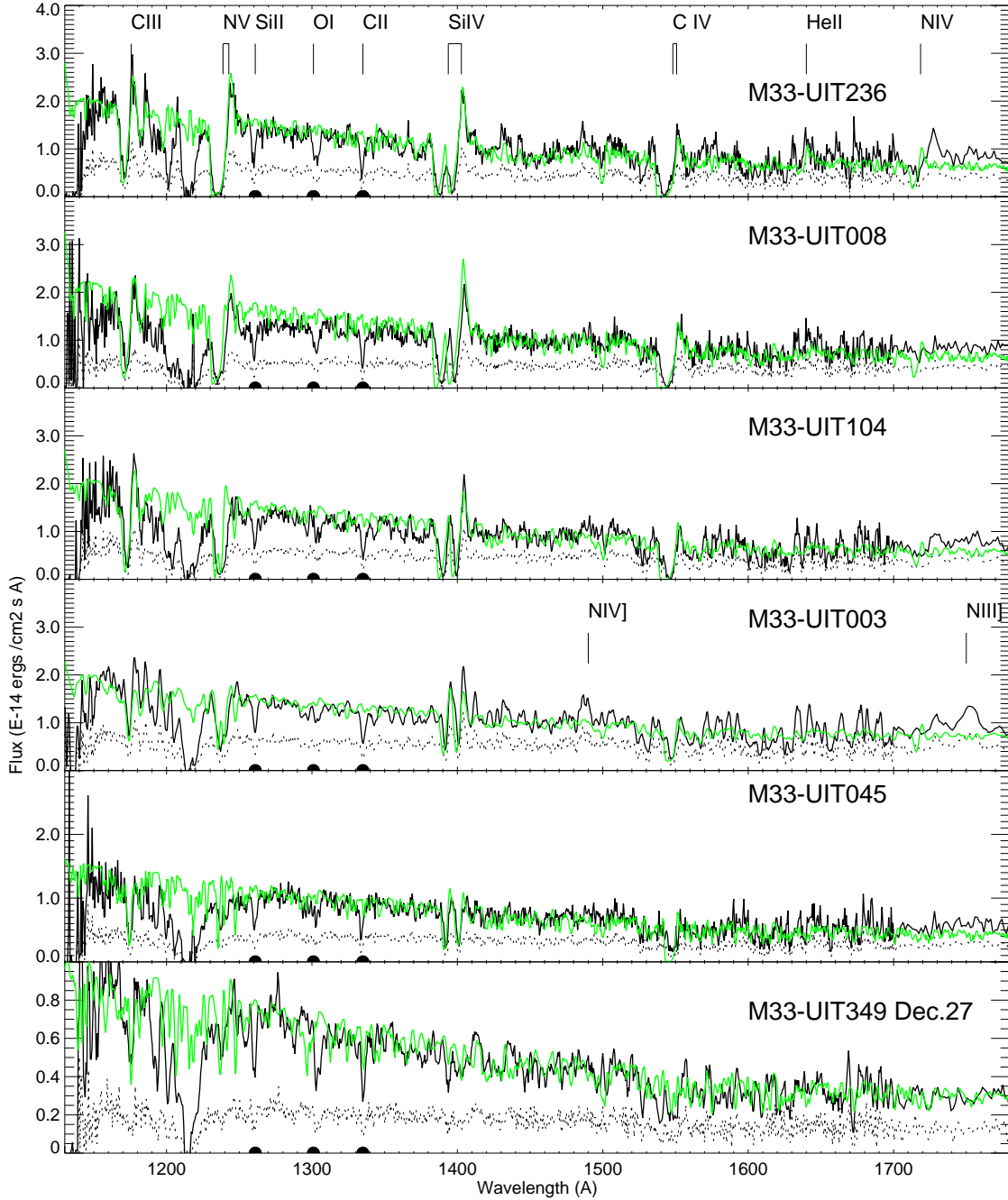


Fig. 6.— The STIS spectra (black line), dereddened for the amount of extinction given in Table 2, and the best fit models (green/light grey) computed with WM-basic. The model parameters are compiled in Table 2. The dotted line is the observed spectrum with no dereddening, to illustrate the sensitivity of our modeling to even such small reddening amounts. The range below 1800Å is shown, where all the strong stellar wind lines are. The strongest interstellar lines in this range, Si II λ 1260, O I λ 1301, and C II λ 1335, are marked with a filled bubble at the bottom of the spectra. In the spectrum of M33-UIT003 two broad emission features are seen, near 1490Å and 1750Å. There are a number of NIV] and NIII] intercombination lines around those wavelengths respectively. The emission is probably not

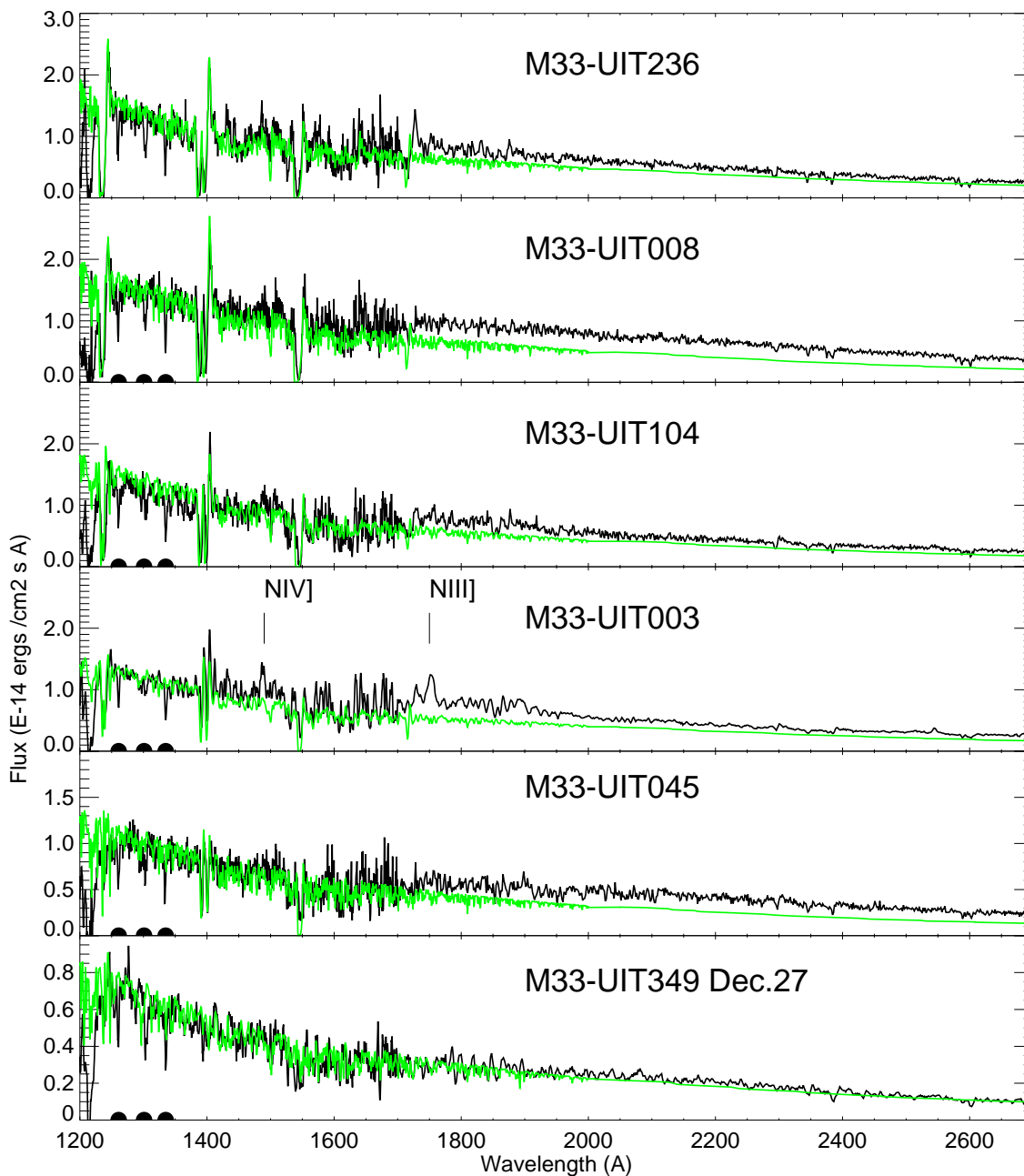


Fig. 7.— Same as in Figure 6, but the longer wavelengths range is shown. The STIS spectra (black line), dereddened for the amount of extinction given in Table 2, and the best fit models computed with WM-basic. A slight flux excess is seen in most spectra beyond $\approx 1800\text{\AA}$, its possible origin is discussed in the text.

Table 1. The program stars and the STIS data

Star name	R.A. (2000)	Dec. (2000)	D_{Gal} [Kpc]	V	B-V	U-B	STIS Data-sets G230L,G140L	M33 velocity [km s ⁻¹]
<i>The Ofpe/WN9 stars</i>								
M33-UIT236	01 33 53.58	30 38 51.8	0.4	18.08	-0.14	-0.84	O5CO04010,20,30	-165.7
M33-UIT008	01 32 45.38	30 38 58.6	6.0	17.67	-0.07	-1.01	O5CO05010,20,30	-145.4
M33-UIT104	01 33 27.22	30 39 09.1	2.1	18.03	-0.14	-0.91	O5CO03010,20,30	-147.5
M33-UIT003	01 32 37.70	30 40 05.7	6.8	17.44	0.01	-0.98	O5CO08010,20,30	-151.1
M33-UIT349	01 34 18.66	30 34 11.6	3.5	18.71	0.57	-0.83	O5CO07010,20,30	-153.0
M33-UIT045	01 33 09.10	30 49 54.5	5.8	18.02	0.00	-1.01	O5CO01010,20,30	-215.9
<i>Serendipitous sources</i>								
M33-UIT349-B	01 34 19.66	30 34 11.6	3.5	O5CO06010,20,30	-153.0
M33-UIT339	01 34 16.06	30 36 42.3	2.8	18.03	0.01	-0.83	O5CO02010,20,30	-173.4
M33-UIT340	01 34 16.04	30 36 38.0	2.8	18.42	-0.04	-0.81	O5CO02010,20,30	-173.4

Table 2. The derived stellar parameters

Star name	E(B-V) [mag]	V_∞ km s ⁻¹	T_{eff} [K]	log g	L/L _⊙	R/R _⊙	\dot{M} [M _⊙ yr ⁻¹]	L_x/L_\odot	M [M _⊙]	[C]/[C _⊙]	[N]/[N _⊙]	C/N (by mass)
M33-UIT236	0.10	1950±150	33,000±1500	3.2	5.67	21	8.e-6	-7.5	26	0.05	10.	0.02
M33-UIT008	0.08	1950±150	32,000±1000	3.2	5.66	22	4.e-6	-7.75	28	0.05	10.	0.02
M33-UIT104	0.09	1600±150	31,000±1500	3.2	5.61	22	3e-6	-8.0	28	0.50	2.	0.90
M33-UIT003	0.07	1000±120	30,000±1500	3.2	5.55	22.	2e-6	-10.	28	0.05	10.	0.02
M33-UIT045	0.10	950±100	30,000±1500	3.2	5.47	20	5e-7	-9.5	23	0.5	0.1::	17::
M33-UIT349	0.11	1700:	27,000±2000:	3.0:	5.28:	20:	1e-8:	-7.0:	15:	0.5:	2.:	0.90